Rare Met. (2022) 41(2):689–699
https://doi.org/10.1007/s12598-021-01808-y

RARE METALS

ORIGINAL ARTICLE

Antibacterial ability and biocompatibility of fluorinated titanium by plasma-based surface modification

Mian Chen*, Xiao-Qiao Wang, Er-Lin Zhang, Yi-Zao Wan, Jian Hu*

Received: 28 April 2021 / Revised: 26 May 2021 / Accepted: 30 May 2021 / Published online: 19 August 2021

Abstract Biomaterial surfaces with satisfied antibacterial activity and appropriate cytocompatibility are a pressing clinical need for orthopedic and dental implants. Fluorine-containing biomaterials have been demonstrated to obtain antibacterial activity and osteogenic property, while the effect of fluorine chemical compositions on antibacterial property and cytocompatibility is rarely studied. To this end, the coatings with different fluorine chemical compositions on titanium surface were prepared by plasma treatment to verify the antibacterial ability and cytocompatibility of fluorinated surfaces. Their antibacterial ability was evaluated by using *Staphylococcus aureus*, and the cell compatibility was investigated with MC3T3-E1 cells in vitro. The results show that both fluorocarbon coating and metal fluorides coating exhibited a hydrophilic and nano-scaled roughness. Rather than the fluorocarbon coating, the coating composed of metal fluorides presented satisfied bactericide effect and excellent cytocompatibility. The antibacterial mechanism is associated with the metal fluorides and released fluoride ion. This work would provide novel sight in optimizing the surface modification method of fluorinated biomaterials for biomedical applications.

M. Chen*, X.-Q. Wang, Y.-Z. Wan, J. Hu*
Jiangxi Key Laboratory of Nanobiomaterials, Institute of Advanced Materials, East China Jiaotong University, Nanchang 330013, China
e-mail: chenmian2016@163.com

J. Hu
e-mail: 642688789@qq.com

E.-L. Zhang
Key Laboratory for Anisotropy and Texture of Materials (ATM), School of Material Science and Engineering, Northeastern University, Shenyang 110819, China

Keywords Titanium; Plasma-based technology; Fluorine; Antibacterial property; Cytocompatibility

1 Introduction

Among metallic biomaterials for orthopedic and dental implants, titanium and its alloys are widely used because of their good biocompatibility, mechanical properties, and great corrosion resistance in the physiological environment [1], while titanium does not have intrinsic antibacterial characteristics and bacterial infection is one of the most serious complications after surgery nowadays [2, 3]. It has been reported that 90% and 50% of all implants showed signs of inflammation and irreversible tissue destruction, respectively [4]. For dental implants, a mean prevalence of peri-implantitis was 22% [5], and the infection rates of peri-prosthetic joint infections were 0.5%–2% [6], 2%–9% [7], and 0.3%–1.7% [8] after total joint replacement of the knee, hip, and ankle, respectively. In particular, *Staphylococcus aureus* (*S. aureus*) was the most common pathogen [8]. Bacterial infections associated with implants are a critical complication that often leads to further surgical intervention and even cause the failure of the implants [9]. Therefore, altering the inert biomaterial surface characteristics by surface modification should be an interesting and primary strategy to prevent implant-related infection.

Over the past decades, several antibacterial reagents have been incorporated to titanium surface to enhance its antibacterial properties, such as Ag nanoparticles [10, 11], Cu^{2+} [12], and Zn^{2+} [13], while the long-term biological safety of metal ions in vivo still needs to be verified. Fluorine, as a necessary trace element in the human body, has been widely used to prevent dental caries in clinics due

to its good antibacterial activity [14]. Meanwhile, various surface modification approaches have been applied to convert the surfaces of biomedical devices into antimicrobial surfaces with fluorine elements, including plasma-based treatment [15] and anodizing [16, 17]. Moreover, the fluorine-containing biomaterials have been confirmed to stimulate osteoblastic activities in terms of cell proliferation and differentiation in vitro and even promote osteoblastic bone formation in vivo [18, 19]. Therefore, modifying titanium surface with fluorine should be a potential way to endow it with improved antibacterial properties and even contribute to bone formation.

Recently, plasma-based technology has attracted much attention to prepare the functional coatings due to that it has the potential to change the physicochemical properties of implant surfaces. Plasma treatment can clean titanium surfaces [20] and increase surface hydrophilicity [21, 22], thereby being able to improve the adhesion and spreading of osteoblastic cells on titanium surfaces [21]. Meanwhile, the advantage of low-temperature operation can guarantee some low-temperature film structures [23]. In our previous study, fluorine has been incorporated on titanium to obtain antibacterial activity and cytocompatibility by plasma-based method. The antibacterial property was enhanced with the fluorination level (composed of titanium fluorides) of titanium surface with the fluoride ion release concentration increasing [24]. However, due to the strong electronegativity of the fluorine atom, the material surface was prone to cover with the polymer-like films composed by CF_x groups during the plasma process. Interestingly, it has been reported that the CF_x-modified surface obtained antibacterial properties and satisfied cytocompatibility due to its low surface energy [25], such as fluorine incorporated diamond-like carbon (F-DLC) films [26, 27] and fluorinated graphene [28]. The antibacterial property was enhanced with the fluorine content [27], while other reports demonstrated that the CF_x films only obtain strong antibacterial properties when incorporated with strong antibacterial regent of nitric oxide [29]. All these contradictory results suggested that the antibacterial property of fluorine-containing material surface was not only related to the fluorine content but also closely related to the fluorine chemical compositions.

With the consideration of above results, in this work, the coatings with different fluorine chemical compositions on titanium surfaces were prepared by plasma-based deposition method to verify the antimicrobial property and cytocompatibility of fluorination surfaces. Their antibacterial ability against *S. aureus* was evaluated by using plate colony-counting method, live/dead bacterial staining, and scanning electron microscopy (SEM) observation, and the cell compatibility was investigated with MC3T3-E1 cells in vitro. This work may provide novel sight in surface modification method of fluorine-containing biomaterials for biomedical applications.

2 Experimental

2.1 Samples preparation

Titanium discs (cp-Ti, Grade 2, Xi'an Saite Metal Materials Development Co. Ltd, China) with the thickness of 2 mm and diameter of 15 mm were used in this experiment. The samples were mechanically ground with silicon carbide papers and polished with diamond suspension, then ultrasonically cleaned and dried for further surface treatment. The pre-treated samples were modified by a plasma treatment system [30]. The detailed parameters of plasma treatment are listed in Table 1. Before the plasma treatment, samples were sputtering with argon plasma for 2 min to clean the sample surface. CF_4 and O_2 were used as the fluorine and oxygen source. The obtained samples are designed as TiF-I and TiF-II, respectively.

2.2 Material characterization

2.2.1 Surface topography and chemical compositions

Field-emission scanning electron microscopy (SEM, JSM-7001F, JEOL, Japan) and atomic force microscopy (AFM, Dimension, Bruke, Germany) were applied to assess the surface morphology and roughness of TiF samples. The fluorine chemical compositions of the TiF coatings were determined by X-ray photoelectron spectroscopy (XPS, Thermo Scientific^{TM}, USA) with sputtering rate of 0.1 nm·s^{-1}.

2.2.2 Contact angle

The water contact angles of different TiF surfaces were determined with an optical contact angle instrument

Table 1 Parameters of plasma treatment

Parameters	TiF-I	TiF-II
Peak power/W	100	300
Bias voltage/V	0	− 500
Gas pressure/Pa	30	30
Gas rate/(ml·min^{-1})		
Ar/(ml·min^{-1})	15	10
CF_4/(ml·min^{-1})	15	5
O_2/(ml·min^{-1})	0	10
Treat time/min	20	20

(SL200KS, Kino, USA) by vertically dropping 3 μl deionized water onto each surface.

2.2.3 Fluoride ion release

Immersion tests were carried out in physiological saline (PS) with an area/volume ratio of 1 cm^2/2.8 ml at 37 °C according to the National Standard of China GB/T 16,886.12, the PS changed every day. The concentration of fluoride ion in daily liquid was examined by ion chromatography (ICS-2100, ThermoFisher, USA).

2.3 Antibacterial assay

Gram-positive *S. aureus* (ATCC 6538) provided by the Center for Typical Culture Collection of China was chosen to assess the antibacterial ability of TiF samples. The bacteria strain was prepared at a concentration of 1×10^7 CFU·ml^{-1} in Lysogeny broth (LB) medium m (1% tryptone, 0.3% yeast extract, 0.5% NaCl; *w*/*v*) and diluted to a concentration of 1×10^5 CFU·ml^{-1} with PS. The samples were placed on a 12 well plate, and 100 μl *S. aureus* suspension was seeded on each sample and incubated at 37 °C.

2.3.1 Quantitative assessment

The plate colony-counting method was used to assess the quantitative antibacterial property. Briefly, after cultured for 24 h, 2 ml PS was added to each well and vortexed for 2 min. Afterward, 100 μl bacterial suspension was collected and inoculated into a standard agar culture plate. Then further incubated at 37 °C for 24 h, the active bacteria were counted and the antibacterial rate (AR) was calculated using the following formula:

$$\mathrm{AR} = \left(N_{\mathrm{control}} - N_{\mathrm{sample}}\right) / N_{\mathrm{control}} \times 100\% \quad (1)$$

where N_{control} and N_{sample} are the bacterial colony number on the cp-Ti and TiF samples, respectively. In order to evaluate the long-lasting antibacterial property, samples were immersed in PS for 1, 3 and 7 days and the degraded AR was assessed by plate colony-counting method as mentioned before.

2.3.2 Bacteria live/dead staining

After cultured for 24 h, live/dead BacLight kit (L13152, Invitrogen, USA) was further applied to further assess the bacteria viability according to the instrument [24]. The imaging of bacteria on different surfaces was carried out via fluorescence microscope (FCS, 90i, Nikon, Japan).

2.3.3 Morphology of bacteria

After cultured for 24 h, glutaraldehyde solution (2.5 vol%) was used to fix the bacteria. Afterward, the bacteria were dehydrated in a graded ethanol series (30%, 50%, 75%, 90%, 95% and 100%; *v*/*v*), freeze-dried, and sputter coated with gold. The morphology of *S. aureus* was examined by SEM.

2.4 Cytocompatibility assay

Mouse pre-osteoblasts cell (MC3T3-E1) was selected to investigate the cytocompatibility of samples. The cells were cultured in a dish with the medium composed of α-MEM (HyClone, USA) containing 10% fetal bovine serum (HyClone, USA) and 1% penicillin–streptomycin (HyClone, USA) in an incubator containing 5% CO_2 at 37 °C. Cells were seeded at a density of 2×10^4 cells·$well^{-1}$ with sterilized samples pre-placed in a 24 well plate.

2.4.1 Cell initial adhesion

After cultured for 1, 4 and 24 h, the cells were washed by phosphate-buffered saline (PBS, HyClone, USA), then fixed with 4% paraformaldehyde (Sigma-Aldrich, USA) for 20 min followed by permeabilized with 0.5% Triton X-100 (Beyotime, China) for 5 min. Afterward, cells were double stained by rhodamine phalloidin (Sigma-Aldrich, USA) and 4,6-diamidino-2-phenylindole (DAPI, Sigma-Aldrich, USA) solution. The cell F-actin and nuclei were finally observed by FCS.

2.4.2 Cell proliferation and morphology

After cultured for 1, 3 and 7 days, the cells were rinsed with PBS twice followed by incubated with 300 μl 10% cell counting Kit-8 (CCK-8, Beyotime, China) medium for 2 h at 37 °C in the dark. Then, 100 μl culture medium was collected to a new 96-well plate and the optical density (OD) was determined at 450 nm on a microplate reader (Infinite 200, Tecan, Switzerland). For cytotoxicity evaluation, the cells relative viability (RV) was calculated using the following formula:

$$\mathrm{RV} = \left(\mathrm{OD}_{\mathrm{sample}} - \mathrm{OD}_{\mathrm{blank}}\right) / \left(\mathrm{OD}_{\mathrm{control}} - \mathrm{OD}_{\mathrm{blank}}\right) \times 100\% \quad (2)$$

For cell morphology observation, the cells were fixed with 2.5% glutaraldehyde after cultured for 1 and 3 days. Afterward, cells were dehydrated and observed by SEM as the protocols displayed in antibacterial test.

2.5 Statistical analysis

The experimental results were expressed as mean ± standard deviations (SD) and compared according to fisher's least significant difference in one-way analysis of variance. $p < 0.05$ was considered to be statistically significant.

3 Results

3.1 Characterization of samples

The detailed morphology of the cp-Ti and TiF samples obtained by SEM is exhibited in Fig. 1a–c. The surface of cp-Ti was smooth although little small grind defects can be observed. In contrast, TiF-I samples show a uniformly nano-raised structure (50 – 100 nm in dimension), while countless of nano-pits (100 – 200 nm in dimension) emerge on TiF-II samples. The fluorine peak has been detected by the corresponding energy dispersive spectroscopy (EDS) area test of TiF samples (Fig. 1g), but it is worth noticing that the EDS quantitative analysis is not precise for the light elements; therefore, other technologies are needed to further analyze the composition of TiF samples. The higher magnified AFM images (Fig. 1d–f) of TiF samples show more details of the microstructures of TiF samples. The surface of TiF-I samples presented large number of nanoparticles with diameter of 50 nm, while the surface TiF-II samples displayed countless nano-pits, and the roughness results (Fig. 1h) show that the TiF-II surfaces exhibited relatively higher surface roughness.

XPS was further performed to probe the chemical compositions throughout the coatings. Figure 1i shows the top XPS survey spectra of cp-Ti and TiF samples; it can be seen that after plasma treatment, a new peak of fluorine appeared and the F 1s intensity of TiF-I samples was much

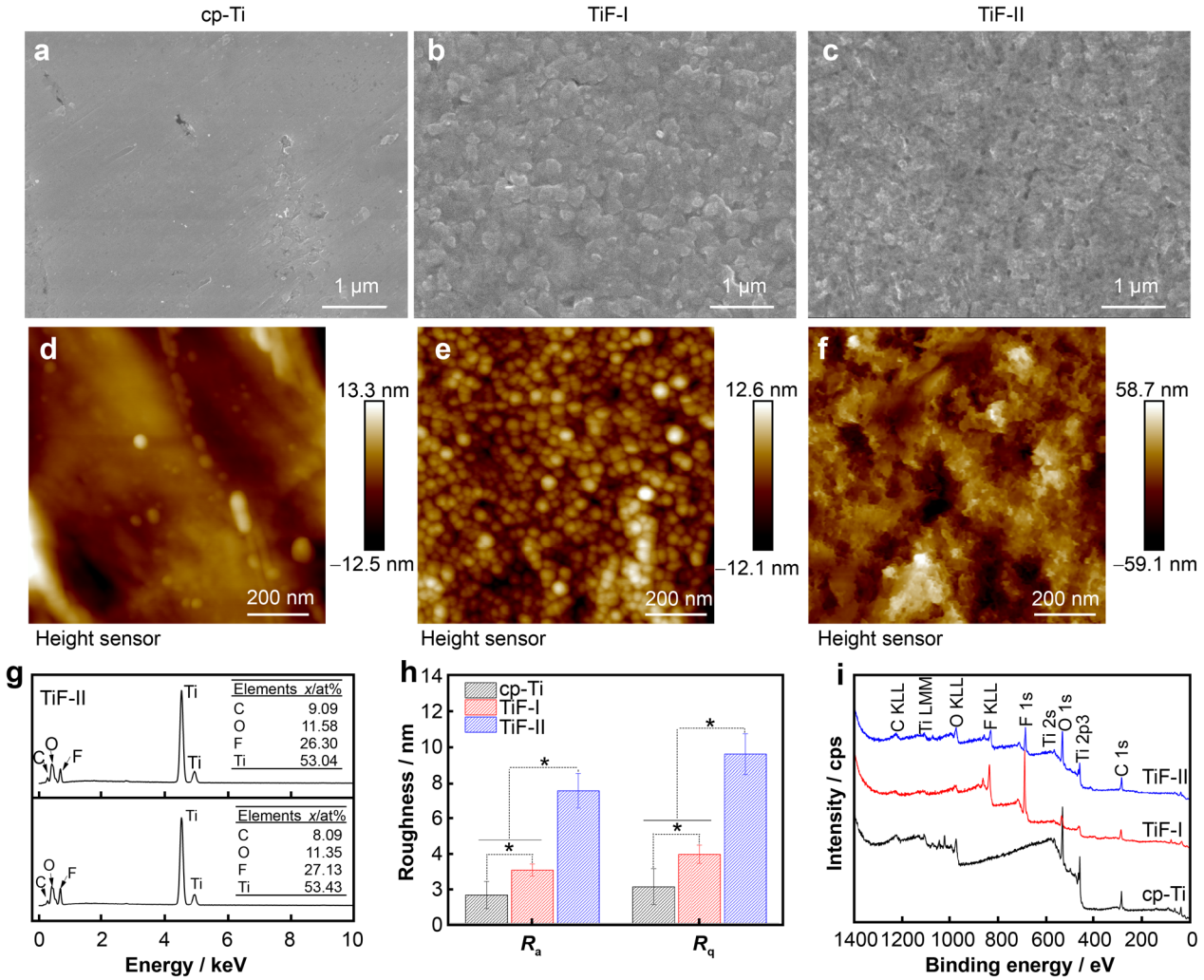

Fig. 1 Surface characterization of cp-Ti and TiF samples: **a-c** SEM images; **d-f** AFM topography; **g** corresponding EDS results; **h** corresponding roughness results; **i** XPS survey spectra of samples' top surface (*$p < 0.05$)

higher than that of TiF-II samples. The influence of plasma fluorination on the chemical compositions of the coating was further investigated with XPS high-resolution of C 1s, O 1s, F 1s, and Ti 2p at different depths (Fig. 2). The C 1s high-resolution spectra of TiF-II samples show that the main components of the surface were C–C/C–H with the binding energy (BE) of 284.6 eV. While the TiF-I exhibited a high proportion of CF_2 and CF_3 components, suggesting that a polymerized CF_x coating was formed on the surface. Meanwhile, the F 1s high-resolution spectra revealed that the organic fluorine with BE of 688–689 eV was mainly observed on TiF-I samples; in contrast, the metal fluorides were formed on TiF-II sample with corresponding BE of 684–685.5 eV. Furthermore, the O 1s high-resolution spectra confirmed that the surface of TiF-I and TiF-II samples was mainly composed of metal oxides with corresponding BE of 529–530 eV. These suggest that higher power energy with excessive oxygen amount during the plasma treatment is prone to form metal fluorides on the surface; otherwise, the surface is easy to be polymerized with fluorocarbons.

To have a better understanding of the interface, the evolution of Ti 2p spectra was fitted to clarify the detained metal fluorides and metal oxides on the samples' surface. For TiF-I samples, the fitting results show that the composition of the outermost surface was TiO_2. After etched by 200 s, pure Ti and titanium-oxide mixtures (TiO_2, Ti_2O_3, TiO) were detected. In contrast, the outermost surface layer of TiF-II samples was composed of TiO_2, Ti_2O_3 along with a small amount of TiF_3. After etched for 200 s, the fitting results of curve present that the TiF-II samples surface composed of a complex chemical structure: TiO_2, Ti_2O_3, TiO, TiF_4 and Ti. These suggest that TiF_3 and TiF_4 compounds are the main fluorinated components of the TiF-II coatings. From the above analysis, it can be concluded that the coatings with different fluorine chemical compositions on titanium have been prepared by plasma treatment, in which the surface of TiF-I samples is mainly composed by the polymerized CF_x coating, while the metal fluoride is the mainly fluorinated components of TiF-II samples.

Figure 3a shows the water contact angle (WCA) change tendency of the TiF surfaces after storage in the atmosphere for different days. The WCA of polished cp-Ti remained at 60° throughout the whole storage period. In contrast, the WCA rapidly declined to below 20° after plasma treatment, suggesting that the fresh prepared TiF surface exhibits a hydrophilic surface. While the WCA increased as the storage time extended, the WCA of TiF-II samples gradually returned to about 60° at the sixth day.

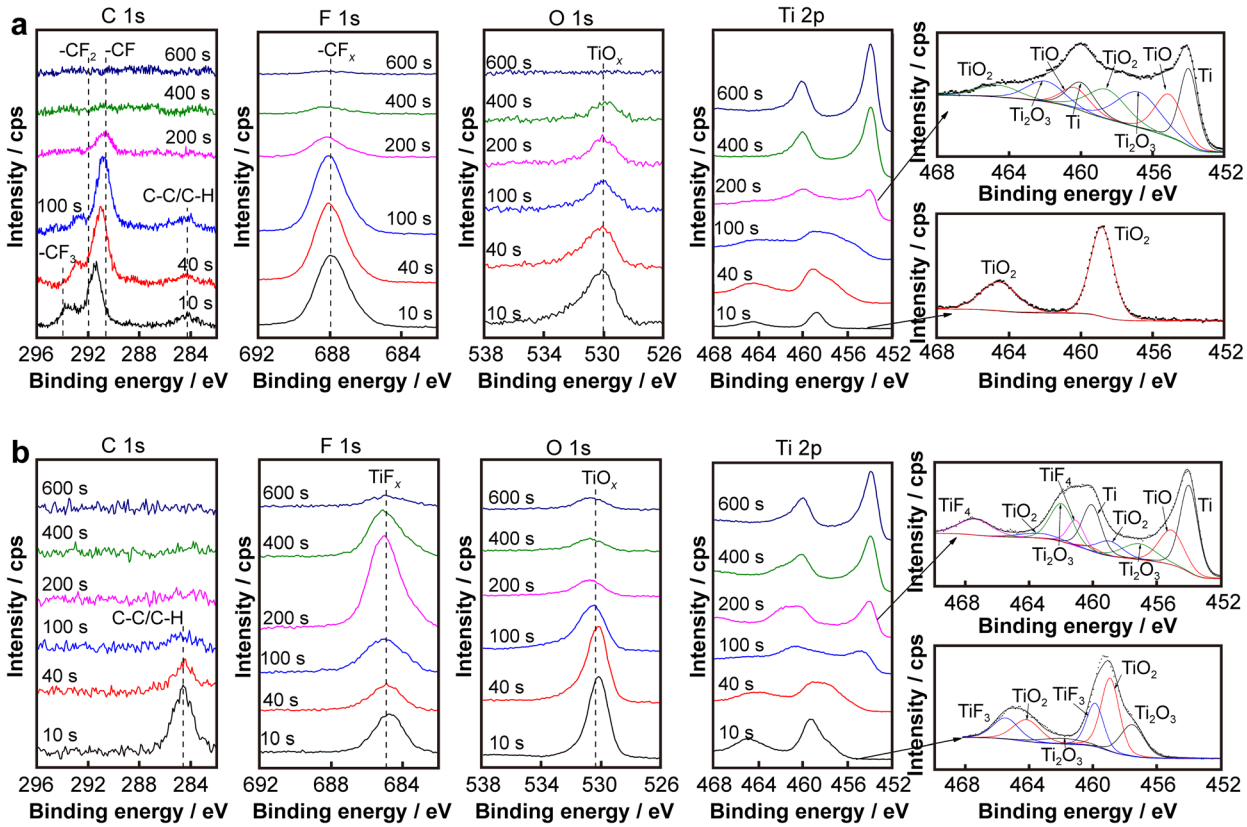

Fig. 2 XPS high-resolution spectra of C 1s, F 1s, O 1s, and Ti 2p of TiF samples: **a** TiF-I samples; **b** TiF-II samples

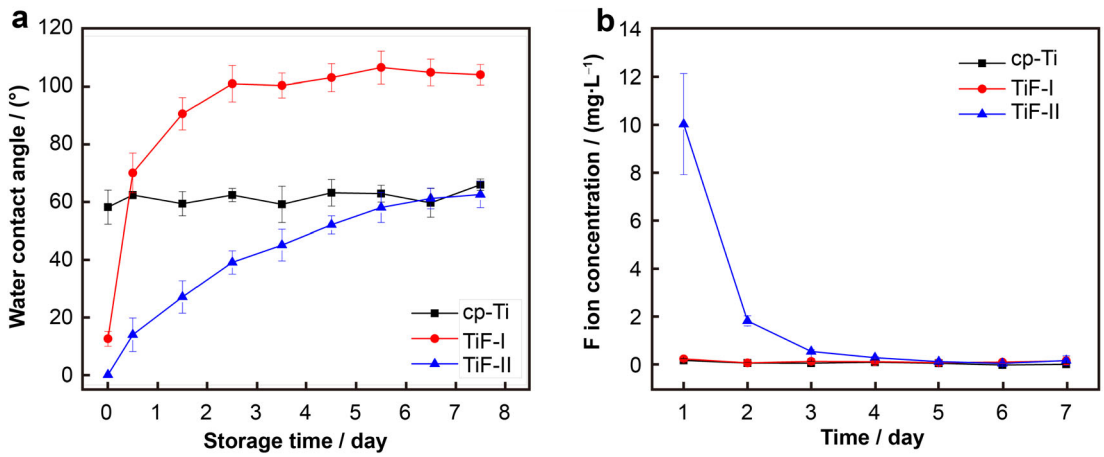

Fig. 3 **a** Water contact angle change tendency of TiF surfaces after storage in the atmosphere for different days; **b** daily fluoride ions release from TiF samples in PS

Nevertheless, the TiF-I surface converted to hydrophobic with the WCA of 112° at the third day. The fluoride ion release test results (Fig. 3b) show that released fluoride ions were only examined in TiF-II samples with a concentration of 10.03 mg·L^{-1} at the first day. Then, the concentration of released fluoride ions reduced rapidly to 1.85 mg·L^{-1} at the second day and continually reduced on the next days. At the sixth day, the concentration of released fluoride ions was undetectable (below the detect limitation of 20 μg·L^{-1}).

3.2 Antibacterial Property

The representative *S. aureus* colonies (Fig. 4a) and antibacterial rate (Fig. 4b) were quantitatively evaluated by the plate colony-counting method. Plenty of bacterial colonies existed on cp-Ti and TiF-I samples, while fewer bacterium left on the TiF-II samples and the corresponding antibacterial rate value reached 93.7%, indicating that the fresh TiF-II samples obtain satisfied antibacterial property compared with TiF-I samples. After immersion in the PS for different days, more bacterium left on the TiF-II samples and the corresponding antibacterial rate value was 82.1%, 73.1% and 70.2% at the first, third and seventh day, respectively. The result suggested that the antibacterial property of TiF sample will degrade after immersion while still can inhibit the bacteria proliferation to some extent.

Live/dead bacterial staining results (Fig. 5a) show that a large number of live *S. aureus* (stained by green) were observed on cp-Ti and TiF-I surfaces, and dead bacteria (stained by red) were hardly found. In contrast, the number of live bacteria decelerated with more dead bacteria detected simultaneously on TiF-II sample surface. The results suggest that the TiF-II surfaces effectively prevented the proliferation of *S. aureus* during the 24 h culturing period. The above results were further confirmed by bacteria morphology observation (Fig. 5b). The low magnification image shows that plenty of *S. aureus* attached,

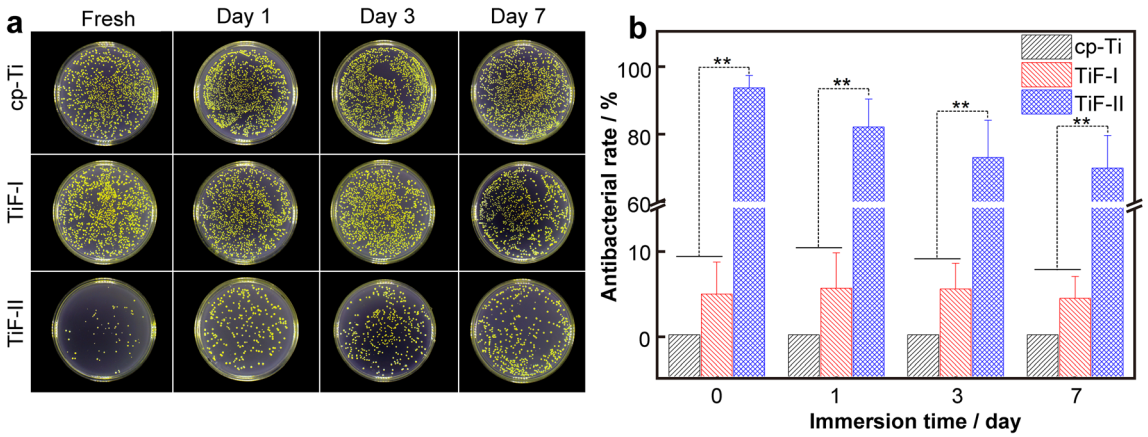

Fig. 4 **a** Recultivated representative *S. aureus* colonies on agar and **b** corresponding antibacterial rates of cp-Ti and TiF samples (**$p < 0.01$)

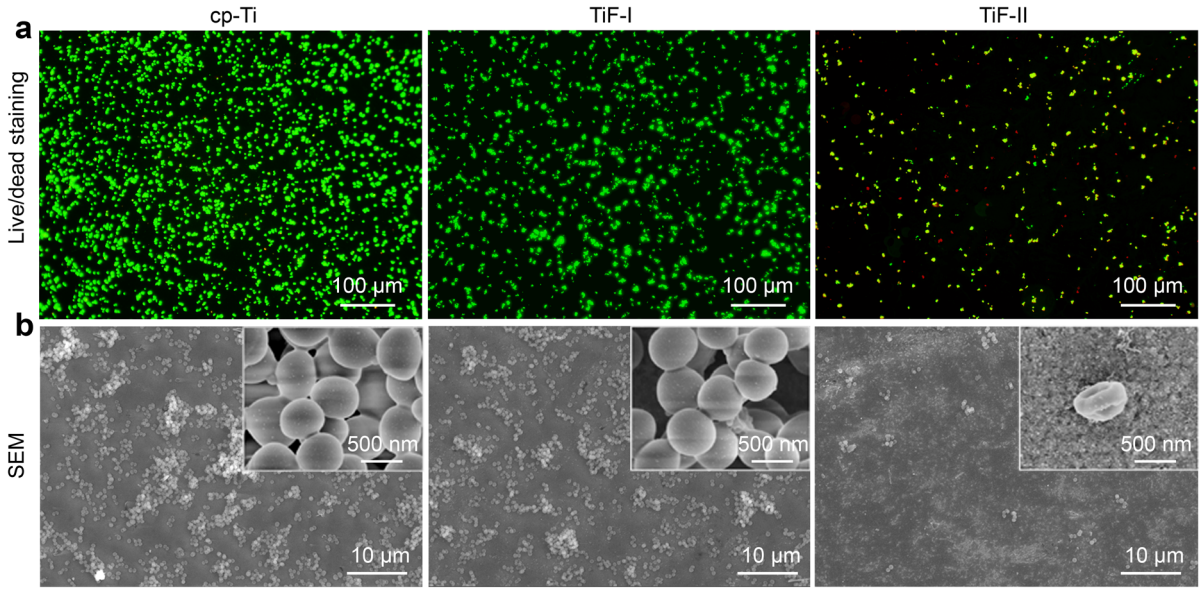

Fig. 5 **a** Fluorescent microscopic images of the live/dead staining and **b** SEM images of *S. aureus* after cultured on cp-Ti and TiF surfaces for 24 h

proliferated, and formed biofilms on the cp-Ti and TiF-I surfaces. The magnified images show the bacteria on cp-Ti and TiF-I surfaces presented typical round cell morphology with a smooth surface. In contrast, the number of *S. aureus* significantly declined and the morphologies were irregular with ruptured bacterial membrane on TiF-II surface.

3.3 Cytocompatibility

The fluorescent staining results (Fig. 6) of rhodamine phalloidin (stained by red) and DAPI (stained by blue) show that the cells on all samples presented sphere morphology at 1 h. After cultured for 4 h, the cells showed obvious spindle morphology with many filopodia on both cp-Ti and TiF samples. Prolonging to 24 h, the cells presented a fibrous structure with apparent F-actin, filopodia, and lamellipodia observed on the cp-Ti and TiF samples. Interestingly, some of the cells spread out larger areas on the TiF-II surface. All these suggest that the TiF samples are biocompatible and the initial attachment behavior of MC3T3-E1 cells can be best promoted by TiF-II samples.

The CCK-8 test results (Fig. 7a, b) show the cells proliferated well during the 7 days culturing period and did not show a statistical difference in the cell proliferation of cp-Ti and TiF samples. The calculated cell viability of TiF samples was all above 75%, indicating no material cytotoxicity of TiF samples. The cell adhesion and proliferation were further evaluated by SEM (Fig. 7c). At the first day, the cells on cp-Ti and TiF-I samples showed a slender shape, while those on TiF-II samples were spread larger, exhibiting a typical polygonal shape with protruded filopodia and lamellipodia. By prolonging the culture time to 3 days, the cp-Ti and TiF surfaces were almost completely covered by cells and the difference in the cell morphology of cp-Ti and TiF samples became unremarkable. The above results suggest that the TiF samples possess good biocompatibility with no significant cytotoxic effect to MC3T3-E1 cells, especially for TiF-II samples, they can even improve the attachment and spread ability of MC3T3-E1 cells.

4 Discussion

Antibacterial capability and cytocompatibility play a critical role in the success of orthopedic and dental implants [31, 32], and the surface composition of the biomaterials is an important factor. Fluorine has been loaded on biomaterials to endow them with sustainable antibacterial properties during the last decades [15, 26], while the controversial results of antibacterial ability to fluorine-containing material surface demonstrate the necessity of investigating the fluorine chemical compositions on bactericide effects. To this end, we attempted to modify the titanium surface with different fluorine chemical compositions by plasma-based technology. During the plasma, the higher peak power could dissociate more reactive fluorine atom and titanium atom [33]; on the other hand, the excessive atomic oxygen could aid dissociate the strong polar C–F bonds and form gaseous CO_2 [34]. These suggest that the competing reactions among titanium atom, fluorine atom, and oxygen atom can be adjusted by varying

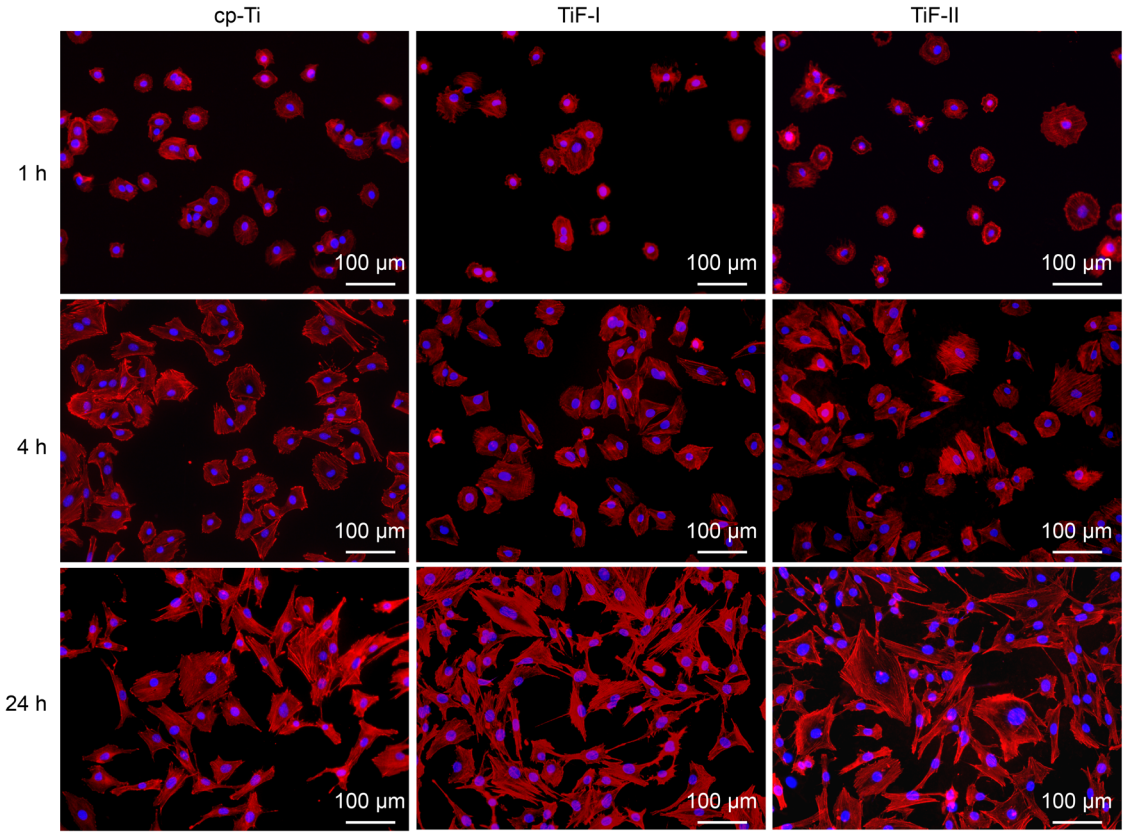

Fig. 6 Fluorescent images of cells cultured on different samples for 1, 4 and 24 h

the peak power and gas amount. Therefore, different plasma parameters were adopted on titanium surfaces to fabricate the surface with different fluorine chemical compositions, and their antibacterial property and cytocompatibility were investigated.

In this work, XPS analysis results determined that the coatings with different surface chemistries were fabricated on substrate. The surface of TiF-I samples is mainly composed of the polymerized CF_x coating, while the metal fluoride is the mainly fluorinated component of TiF-II samples. Besides, SEM and AFM results also confirmed that the surface morphology and roughness of TiF-I and TiF-II samples are much different, in which TiF-I samples presented a nano-convex texture surface, while TiF-II surface exhibited countless nano-pits and relative higher roughness. Furthermore, the plasma-treated fresh surface all showed a hydrophilic surface. Normally, the plasma treatment could modify either polymers or metal materials surface to hydrophilic [35]. While the surface hydrophilicity degraded as the storage time extension, this should be attributed to the fact that the surface defects after plasma treatment were replaced gradually by oxygen atoms from the atmosphere [21, 35]. Moreover, the presence of fluorocarbon on TiF-I surfaces can effectively convert the surface wettability from hydrophilic to hydrophobic [27]. The various surface topography, composition, roughness, and hydrophilicity of biomaterials would have a significant impact on further antibacterial property and cytocompatibility.

Up to now, the antibacterial ability of fluorine has been reported by available studies [30, 36]. Among them, most opinions focus on the role of fluoride ions and metal fluoride compounds, which can lead to oxidative stress, prevent bacterial energy metabolism and destroy the bacterial membrane, ultimately resulting in bacteria death [24, 37]. The antibacterial activity results of TiF samples demonstrated that only the TiF-II sample with the surface composition of metal fluorides obtained the antibacterial efficiency, which should be mainly contributed to the fluoride ion release, the subtle dissolution, and ionization in aqueous solution occurring as: $TiF_4(s) \rightarrow Ti^{4+}(aq) + 4F^-(aq)$. Reportedly, the released fluoride ion concentration of 4 $mg \cdot L^{-1}$ can effectively inhibit bacteria adhesion and colonization [19]. The ion release test shows that 10.03 $mg \cdot L^{-1}$ fluoride ions were released from TiF-II surfaces after 24 h immersion, thereby endowing it with the satisfied antibacterial rate ($> 90\%$). Moreover, the existed insoluble TiF_3 compounds on the TiF-II samples surface also can result in bacteria inactivation by causing oxidative stress, which should be the reason of the relative

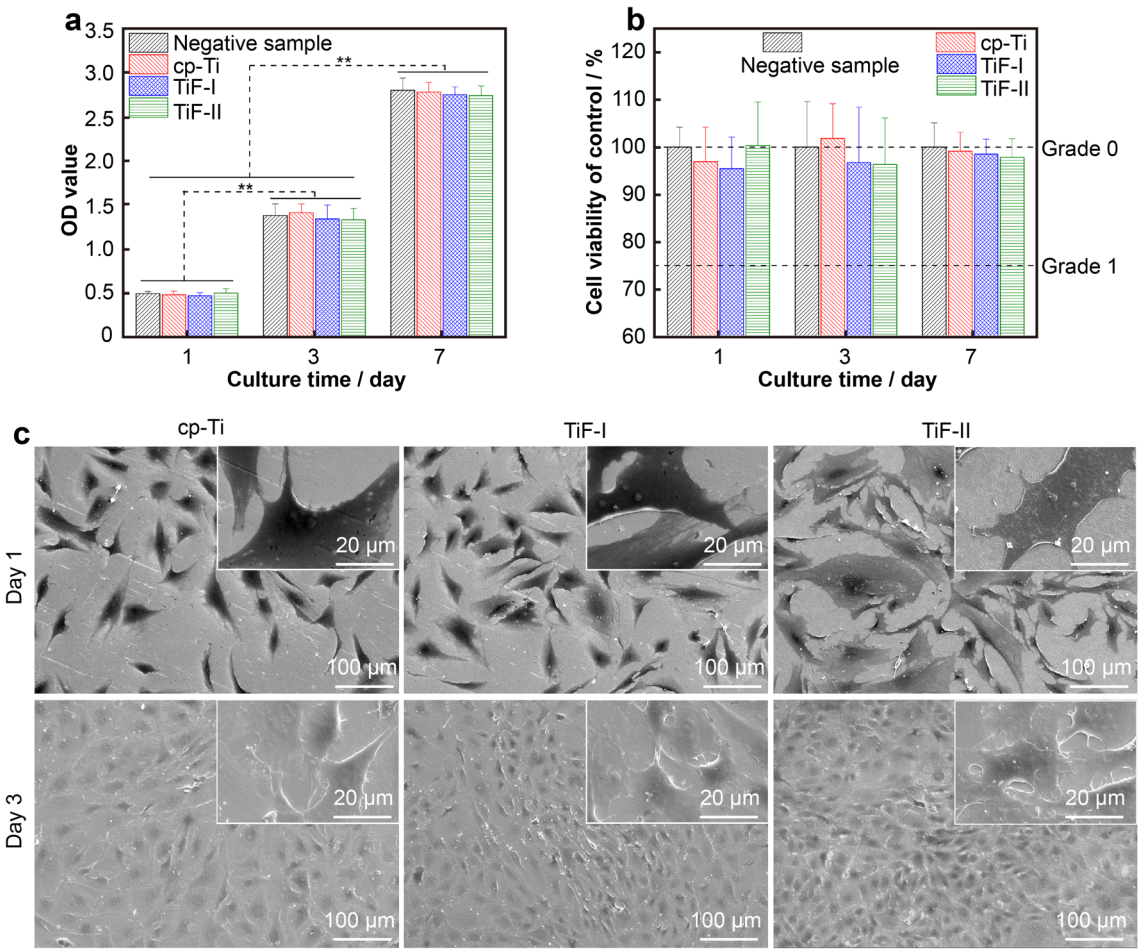

Fig. 7 **a, b** Cell viability evaluated by CCK-8 after cultured for 1, 3 and 7 days (**$p < 0.01$); **c** SEM images of cells cultured on different samples for 1 and 3 days

long-lasting antibacterial property of the TiF-II samples. Nevertheless, other reports also found that the fluorinated hydrophobic surface can effectively prevent bacterial adhesion, proliferation, and thereby inhibiting the formation of infectious biofilms [38, 39]. Besides, rougher and hydrophilic surfaces are more attractive to *S. aureus* bacterial cells and facilitate their adhesion and survival [39, 40]. Generally, the C–F bond is the most inert and resistant to defluorination [41]. All these may be the reason that the hydrophilic TiF-I surface with limited fluoride ion release did not show antibacterial property.

Concerning cell compatibility, it has been reported that micromolar fluoride ion is capable of improving osteoblast adhesion, proliferation, and differentiation activity, while excessive millimolar fluoride ion may lead to cytotoxicity [42–44]. In this study, the concentration of fluoride ion released from TiF-II sample on the first day was 10.03 $mg{\cdot}L^{-1}$, while it significantly decreased to 1.85 $mg{\cdot}L^{-1}$ on the second day and continually reduced till undetectable. Other reports confirmed that osteoblasts can even survive with 1200 $\mu mol{\cdot}L^{-1}$ ($\sim$ 23 $mg{\cdot}L^{-1}$) fluoride ion [43]. Meanwhile, the organofluoride compounds (carbon–fluorine bond), which have been proved to show good biocompatibility, are increasingly used for biomedical devices [18]. The immunofluorescence staining, CCK-8, and SEM observation results confirm that TiF samples possessed good biocompatibility with no significant cytotoxic effect on MC3T3-E1 cells viability, but the TiF-II samples even improved cell attachment and spreading activity. The nanostructured and hydrophilic surfaces of TiF samples may be the other reasons for the benefited cell activities [21, 45]. Although the detailed molecular mechanism still needs to be verified, larger cell spreading with apparent F-actin, filopodia, and lamellipodia expressions is generally considered to facilitate communication between cells and be beneficial to osteoblast differentiation [46, 47]. Additionally, better cell adhesion and spreading on material surface are favorable for the competition of "race for the surface" against bacteria [48], thereby aiding

to fight infection and accelerating the final osseointegration.

Overall, the satisfied bactericide efficiency and excellent cytocompatibility of fluorine-containing titanium surface clarified that the metal fluoride is more sufficient in antibacterial efficiency rather than fluorocarbon. However, the microstructure of TiF samples after immersion is still required to be investigated to clarify the fluoride dissolution kinetics and mechanisms. Moreover, the broad spectra antibacterial ability and molecular long-term antibacterial mechanism are also needed to be investigated in the future to verify the differences of materials against various bacteria strains and the degraded antibacterial property differences of fluorinated coating.

5 Conclusion

The coatings with different fluorine chemical compositions on titanium were successfully prepared by plasma treatment. The peak power and gas amount during the plasma process can effectively influence the chemical compositions of coatings and their properties. Both fluorocarbon coating and metal fluorides coating exhibited a hydrophilic and nano-scaled roughness. Rather than the fluorocarbon coating, the coating composed of metal fluorides presented a satisfied bactericide effect and excellent cytocompatibility. The antibacterial mechanism is associated with the fluoride metals and released fluoride ion. This work would provide novel sight in optimizing the surface modification method of fluorinated biomaterials for orthopedic or dental clinical application.

Acknowledgements This study was financially supported by the National Natural Science Foundation of China (No. 52001122, 51801064 and 51961012), Jiangxi Outstanding Young Talents Program (No. 20192BCB23014), and Jiangxi Key Research and Development Program (No. 20203BBE53050).

Declarations

Conflicts of interests The authors declare that they have no conflict of interests.

References

[1] Zhang E, Zhao X, Hu J, Wang R, Fu S, Qin G. Antibacterial metals and alloys for potential biomedical implants. Bioact Mater. 2021;6(8):2569.
[2] Zhao L, Chu PK, Zhang Y, Wu Z. Antibacterial coatings on titanium implants. J Biomed Mater Res. 2010;91(1b):470.
[3] Neoh KG, Hu X, Zheng D, Kang ET. Balancing osteoblast functions and bacterial adhesion on functionalized titanium surfaces. Biomaterials. 2012;33(10):2813.
[4] Grischke J, Eberhard J, Stiesch M. Antimicrobial dental implant functionalization strategies-a systematic review. Dent Mater J. 2016;35(4):545.
[5] Derks J, Tomasi C. Peri-implant health and disease. A systematic review of current epidemiology. J Clin Periodontol. 2015; 42(Suppl. 16):S158.
[6] Laffer RR, Graber P, Ochsner PE, Zimmerli W. Outcome of prosthetic knee-associated infection: evaluation of 40 consecutive episodes at a single centre. Clin Microbiol Infect. 2006; 12(5):433.
[7] Wu C, Qu X, Liu F, Li H, Mao Y, Zhu Z. Risk factors for periprosthetic joint infection after total hip arthroplasty and total knee arthroplasty in Chinese patients. PLoS One. 2014;9(4): e95300.
[8] Kessler B, Sendi P, Graber P, Knupp M, Zwicky L, Hintermann B, Zimmerli W. Risk factors for periprosthetic ankle joint infection: a case-control study. J Bone Jt Surg. 2012;94(20): 1871.
[9] Liu H, Liu R, Ullah I, Zhang S, Sun Z, Ren L, Yang K. Rough surface of copper-bearing titanium alloy with multifunctions of osteogenic ability and antibacterial activity. J Mater Sci Technol. 2020;48:130.
[10] Zheng Y, Li J, Liu X, Sun J. Antimicrobial and osteogenic effect of Ag-implanted titanium with a nanostructured surface. Int J Nanomed. 2012;7:875.
[11] Wang J, Li J, Qian S, Guo G, Wang Q, Tang J, Shen H, Liu X, Zhang X, Chu PK. Antibacterial surface design of titanium-based biomaterials for enhanced bacteria-killing and cell-assisting functions against periprosthetic joint infection. ACS Appl Mater Interfaces. 2016;8(17):11162.
[12] Wu Q, Li J, Zhang W, Qian H, She W, Pan H, Wen J, Zhang X, Liu X, Jiang X. Antibacterial property, angiogenic and osteogenic activity of Cu-incorporated TiO_2 coating. J Mater Chem B. 2014;2:6738.
[13] Jin G, Cao H, Qiao Y, Meng F, Zhu H, Liu X. Osteogenic activity and antibacterial effect of zinc ion implanted titanium. Colloids Surf B. 2014;117:158.
[14] Liao Y, Brandt BW, Li J, Crielaard W, Loveren CV, Deng DM. Fluoride resistance in *Streptococcus mutans*: a mini review. J Oral Microbiol. 2017;9(1):1344509.
[15] Wang XJ, Liu HY, Ren X, Sun HY, Zhu LY, Ying XX, Hu SH, Qiu ZW, Wang LP, Wang XF, Ma GW. Effects of fluoride-ion-implanted titanium surface on the cytocompatibility in vitro and osseointegatation in vivo for dental implant applications. Colloids Surf B. 2015;136:752.
[16] Perez-Jorge C, Arenas MA, Conde A, Hernández-Lopez JM, Damborenaa JJ, Fisher S, Hunt AMA, Esteban J, James G. Bacterial and fungal biofilm formation on anodized titanium alloys with fluorine. J Mater Sci Mater Med. 2017;28:8.
[17] Ge X, Leng Y, Bao C, Xu SL, Wang R, Ren F. Antibacterial coatings of fluoridated hydroxyapatite for percutaneous implants. J Biomed Mater Res Part A. 2010;95A(2):588.
[18] Wang L, He S, Wu X, Liang S, Mu Z, Wei J, Deng F, Deng Y, Wei S. Polyetheretherketone/nano-fluorohydroxyapatite composite with antimicrobial activity and osseointegration properties. Biomaterials. 2014;35(25):6758.
[19] Guo G, Zhou H, Wang Q, Wang J, Tan J, Li J, Jin P, Shen H. Nano-layered magnesium fluoride reservoirs on biomaterial surfaces strengthen polymorphonuclear leukocyte resistance to bacterial pathogens. Nanoscale. 2016;9(2):875.
[20] Canullo L, Micarelli C, Lembo-Fazio L, Iannello G, Clementini M. Microscopical and microbiologic characterization of customized titanium abutments after different cleaning procedures. Clin Oral Impl Res. 2014;25(3):328.
[21] Duske K, Koban I, Kindel E, Schröder K, Nebe B, Holtfreter B, Jablonowski L, Weltmann KD, Kocher T. Atmospheric plasma

enhances wettability and cell spreading on dental implant metals. J Clin Periodontol. 2012;39(4):400.
[22] Koban I, Duske K, Jablonowski L, Schröder K, Nebe B, Sietmann R, Weltmann KD, Hübner NO, Kramer A, Kocher T. Atmospheric plasma enhances wettability and osteoblast spreading on dentin in vitro: proof-of-principle. Plasma Process Polym. 2011;8(10):975.
[23] Chu PK, Chen JY, Wang LP, Huang N. Plasma-surface modification of biomaterials. Mater Sci Eng R. 2002;36(5–6):143.
[24] Chen M, Zhang Y, Fu S, Yang L, Wang X, Wang Q, Qin G, Chen D, Zhang E. Effect of fluorination/oxidation level of nano-structured titanium on the behaviors of bacteria and osteoblasts. Appl Surf Sci. 2020;502:144077.1.
[25] Vassallo E, Pedroni M, Silvetti T, Morandi S, Toffolatti S, Angella G, Brasca M. Bactericidal performance of nanostructured surfaces by fluorocarbon plasma. Mater Sci Eng C. 2017;80:117.
[26] Marciano FR, Lima-Oliveira DA, Da-Silva NS, Corat EJ, Trava-Airoldi VJ. Antibacterial activity of fluorinated diamond-like carbon films produced by PECVD. Surf Coat Technol. 2010;204(18–19):2986.
[27] Ishihara M, Kosaka T, Nakamura T, Tsugawa K, Hasegawa M, Kokai F, Koga Y. Antibacterial activity of fluorine incorporated DLC films, Diamond Relat. Mater. 2006;15(4–8):1011.
[28] Geng H, Wang T, Cao H, Zhu H, Di Z, Liu X. Antibacterial ability, cytocompatibility and hemocompatibility of fluorinated grapheme. Colloids Surf B. 2019;173:681.
[29] Choi M, Park S, Park K, Jeong H, Hong J. Nitric oxide delivery using biocompatible perfluorocarbon microemulsion for antibacterial effect. ACS Biomater Sci Eng. 2019;5(3):1378.
[30] Chen M, Li H, Wang X, Qin G, Zhang E. Improvement in antibacterial properties and cytocompatibility of titanium by fluorine and oxygen dual plasma-based surface modification. Appl Surf Sci. 2019;463:261.
[31] Goodman SB, Yao Z, Keeney M, Yang F. The future of biologic coatings for orthopaedic implants. Biomaterials. 2013;34(13):3174.
[32] Zhang E, Fu S, Wang R, Li H, Liu Y, Ma Z, Liu G, Zhu C, Qin G, Chen D. Role of Cu element in biomedical metal alloy design. Rare Met. 2019;38(6):476.
[33] Lee EJ, Kim JW, Lee WJ. Reactive ion etching mechanism of RuO_2 thin films in oxygen plasma with the addition of CF_4, Cl_2, and N_2. Jpn J Appl Phys. 1998;37(5R):2634.
[34] Fracassi F, d'Agostino R. Chemistry of titanium dry etching in fluorinated and chlorinated gases. Pure Appl Chem. 1992;64(5):703.
[35] Xu LC, Siedlecki CA. *Staphylococcus epidermidis* adhesion on hydrophobic and hydrophilic textured biomaterial surfaces. Biomed Mater. 2014;9(3):035003.
[36] Zhou J, Li B, Zhao L, Zhang L, Han Y. F-doped micropore/nanorod hierarchically patterned coatings for improving antibacterial and osteogenic activities of bone implants in bacteria-infected cases. ACS Biomater Sci Eng. 2017;3(7):1437.
[37] Sutton SVW, Bender GR, Marquis RE. Fluoride inhibition of proton-translocating ATPases of oral bacteria. Infect Immun. 1987;55(11):2597.
[38] Zheng H, Liu L, Meng F, Cui Y, Li Z, Oguzie EE, Wang F. Multifunctional superhydrophobic coatings fabricated from basalt scales on a fluorocarbon coating base. J Mater Sci Technol. 2021;84:86.
[39] Bazaka K, Jacob MV, Crawford RJ, Ivanova EP. Plasma-assisted surface modification of organic biopolymers to prevent bacterial attachment. Acta Biomater. 2011;7(5):2015.
[40] Wang G, Jin W, Qasim AM, Gao A, Peng X, Li W, Feng H, Chu PK. Antibacterial effects of titanium embedded with silver nanoparticles based on electron-transfer-induced reactive oxygen species. Biomaterials. 2017;124:25.
[41] Amii H, Uneyama K. C-F bond activation in organic synthesis. Chem Rev. 2009;109(5):2119.
[42] Everett ET. Fluoride's effects on the formation of teeth and bones, and the influence of genetics. J Dent Res. 2011;90(5):552.
[43] Wu S, Xia B, Mai S, Feng Z, Wang X, Liu Y, Liu R, Li Z, Xiao Y, Chen Z, Chen Z. Sodium fluoride under dose range of 2.4–24 μM, a promising osteoimmunomodulatory agent for vascularized bone formation. ACS Biomater Sci Eng. 2019;5(2):817.
[44] Lau KHW, Baylink DJ. Molecular mechanism of action of fluoride on bone cells. J Bone Miner Res. 1998;13(11):1660.
[45] Lavenus S, Ricquier JC, Louarn G, Layrolle P. Cell interaction with nanopatterned surface of implants. Nanomedicine. 2010;5(6):937.
[46] Civitelli R. Cell–cell communication in the osteoblast/osteocyte lineage. Arch Biochem Biophys. 2008;473(2):188.
[47] Qin H, Cao H, Zhao Y, Jin G, Cheng M, Wang J, Jiang Y, An Z, Zhang X, Liu X. Antimicrobial and osteogenic properties of silver-ion-implanted stainless steel. ACS Appl Mater Interfaces. 2015;7(20):10785.
[48] Gupta A, Bastiampillai T, Adams M, Nelson A, Nance M. Biomaterial-centered infection: microbial adhesion versus tissue integration. Science. 1987;237(10):1588.